Journal of Advanced Ceramics

Volume 5 | Issue 3 Article 4

2016

Superconducting parameter determination for $(Co_{0.5}Zn_{0.5}Fe_2O_4)_x/Cu_{0.5}Tl_{0.5}$-1223 composite

M. ME. BARAKAT
Physics Department, Faculty of Science, Alexandria University, Alexandria, Egypt

N. AL-SAYYED
Physics Department, Faculty of Science, Beirut Arab University, Beirut, Lebanon

R. AWAD
Physics Department, Faculty of Science, Beirut Arab University, Beirut, Lebanon

A. I. ABOU-ALY
Physics Department, Faculty of Science, Alexandria University, Alexandria, Egypt

Journal of Advanced Ceramics
2016, **5**(3): 210–218
DOI: 10.1007/s40145-016-0192-2

ISSN 2226-4108
CN 10-1154/TQ

Research Article

Superconducting parameter determination for $(Co_{0.5}Zn_{0.5}Fe_2O_4)_x/Cu_{0.5}Tl_{0.5}$-1223 composite

M. ME. BARAKAT[a,*], N. AL-SAYYED[b], R. AWAD[b], A. I. ABOU-ALY[a]

[a]*Physics Department*, *Faculty of Science*, *Alexandria University*, *Alexandria*, *Egypt*
[b]*Physics Department*, *Faculty of Science*, *Beirut Arab University*, *Beirut*, *Lebanon*

Received: February 27, 2016; Revised: May 10, 2016; Accepted: May 15, 2016

Abstract: The addition of magnetic $Co_{0.5}Zn_{0.5}Fe_2O_4$ nanoparticles to the superconducting $Cu_{0.5}Tl_{0.5}$-1223 phase has been used to investigate the electrical resistivity behavior of the composite above the superconducting transition temperature T_c. This was studied according to the opening of spin gap and fluctuation conductivity. The results indicated that the pseudogap temperature (T^*) and superconducting fluctuation temperature (T_{scf}) change by increasing the addition of $Co_{0.5}Zn_{0.5}Fe_2O_4$ nanoparticles. It was found that T^* is related to hole carrier concentration P and it also depends on the antiferromagnetic fluctuation affected by magnetic nanoparticles. The excess-conductivity analysis showed four different fluctuation regions started from high temperature up to T_c, and they were denoted by short wave (sw), two-dimensional (2D), three-dimensional (3D), and critical (cr) fluctuations. The crossover temperature between 3D and 2D ($T_{3D–2D}$) in the mean field region was decreased by increasing the addition of $Co_{0.5}Zn_{0.5}Fe_2O_4$ nanoparticles, in accordance with the decrease in T_{scf} with x. The coherence length at 0 K along c-axis $\xi_c(0)$, effective layer thickness of the 2D system d, and inter-layer coupling strength J were estimated as a function of $Co_{0.5}Zn_{0.5}Fe_2O_4$ nanoparticle addition. Moreover, the thermodynamics, lower and upper critical magnetic fields, as well as critical current density have been calculated from the Ginzburg number N_G. It was found that the low concentration of $Co_{0.5}Zn_{0.5}Fe_2O_4$ nanoparticles up to $x = 0.08$ wt% improves the superconducting parameters of $Cu_{0.5}Tl_{0.5}$-1223 phase. On the contrary, these parameters were deteriorated for $(Co_{0.5}Zn_{0.5}Fe_2O_4)_x/Cu_{0.5}Tl_{0.5}$-1223 composite with $x > 0.08$ wt%.

Keywords: $Co_{0.5}Zn_{0.5}Fe_2O_4$ nanoparticles; $Cu_{0.5}Tl_{0.5}$-1223 phase; pseudogap temperature; fluctuation conductivity

1 Introduction

Cu-1223 phase was synthesized at high pressure of 4 GPa with $T_c = 67$ K and anisotropy parameter $\Gamma \approx 1.6$ [1–3]. Unfortunately, the high pressure synthesis hinders this phase from the large scale applications such as superconducting cables and magnets. The partial substitution of thallium at copper site in the charge reservoir layer of Cu-1223 phase develops a new $Cu_{1-x}Tl_x$-1223 phase that can be easily prepared at normal pressure. This is probably due to the hybrid of both Tl and Cu charge in the reservoir layer, leading to moderate synthesis conditions which maintain the low superconducting anisotropy [4]. $Cu_{0.5}Tl_{0.5}$-1223 phase has low anisotropy parameter, high critical current density J_c and T_c [4,5]. Therefore, this phase is a promising candidate for technological applications. The

* Corresponding author.
E-mail: maibarakat_phy@yahoo.com

tetragonal structure of $Cu_{0.5}Tl_{0.5}$-1223 phase belongs to the superconductor cuprate with a *P*4/*mmm* space group. It contains three CuO_2 planes and a semi-insulating charge reservoir layer $(Cu_{0.5}Tl_{0.5})Ba_2O_{4-\delta}$ in the unit cell.

The explanation of electrical resistivity behavior above the superconducting transition temperature is still unclear. Therefore, many studies concerned the deviation from linear behavior at certain temperature above T_c. The excess-conductivity studies, due to thermal fluctuations, are very important for understanding the intrinsic properties and dimensionality of high temperature superconductors (HTSCs). The intrinsic properties such as conduction dimensionality and coherence length, in addition to the extrinsic properties which include the sample's grain morphology, are of great importance in determining the superconducting properties. Several models are used to analyze the excess-conductivity such as Aslamazove–Larkin (AL), Maki–Thompson (MT), Lawrence–Doniach (LD), and Hikami–Larkin (HL) [6–9]. AL and LD models have been used to study the excess-conductivity for $Cu_{0.5}Tl_{0.5}$-1223 phase. Qasim *et al*. [10] studied the excess-conductivity of $Cr_x/Cu_{0.5}Tl_{0.5}$-1223 phase ($x = 0.00$, 0.50, 0.75, and 1.00 wt%). They attributed the change in the superconducting parameters to antiferromagnetic nature of Cr nanoparticles and the oxygen disorder within the superconducting regions which affect the carrier density in CuO_2 planes. Nadeem *et al*. [11] reported the excess-conductivity of $(NiFe_2O_4)_x/Cu_{0.5}Tl_{0.5}$-1223 composite with $x = 0.00$, 0.25, 0.50, and 1.00 wt%. They found that both the superconducting volume fraction and 3D conductivity fluctuation decrease by increasing $NiFe_2O_4$ nanoparticle addition as a result of the localization of carriers across these magnetic nanoparticles. The 3D region shifted towards lower temperature due to the increase in the insulating behavior of the inter-grain boundaries. Hussain *et al*. [12] investigated the excess-conductivity of $Ag_x/Cu_{0.5}Tl_{0.5}$-1223 phase with $x = 0.0$, 0.5, 1.0, 2.0, and 4.0 wt%. The superconducting parameters were improved with the inclusion of Ag nanoparticles. This improvement was discussed according to healing of voids and improving the inter-grain connectivity of $Ag_x/Cu_{0.5}Tl_{0.5}$-1223 composite.

One of the properties of oxygen deficient HTSCs is a pseudogap (PG) which appears at temperature higher than T_c over a certain range of hole carrier concentration, extending from the under-doped to the slightly over-doped regions [13]. This phenomenon is explained according to different reasons such as electron pairing [14,15], antiferromagnetic fluctuation [16], and spin–charge separation scenario [17,18]. There are two main reasons that explain this phenomenon: (1) the first one is based on strong pairing regime with low dimensionality and low superfluid density [14] at which PG arises from strong superconductivity fluctuation; (2) PG could arise from some non-superconducting correlations at which PG competes with superconductivity [19]. Khurram *et al.* [20] reported that the pseudogap temperature is the lowest in $Cu_{0.5}Tl_{0.5}$-1223 sample which has the highest T_c in $Cu_{0.5}Tl_{0.5}$-12(n−1)n family compared with $Cu_{0.5}Tl_{0.5}$-1212 and $Cu_{0.5}Tl_{0.5}$-1234 samples.

In the present work, the temperature dependence of electrical resistivity for $(Co_{0.5}Zn_{0.5}Fe_2O_4)_x/Cu_{0.5}Tl_{0.5}$-1223 composite was performed and analyzed according to the opening of pseudogap spin and fluctuation conductivity. The superconducting parameters such as the coherence length at 0 K along *c*-axis, effective layer thickness of the 2D system, inter-layer coupling strength, the thermodynamics, lower and upper critical magnetic fields, and critical current density were calculated as a function of $Co_{0.5}Zn_{0.5}Fe_2O_4$ nanoparticle addition.

2 Experimental technique

$Co_{0.5}Zn_{0.5}Fe_2O_4$ nanoparticle powder was prepared using co-precipitation method by dissolving pure chemical reagents of $FeCl_3·6H_2O$, $ZnCl_2$, and $CoCl_2·6H_2O$ in distilled water, and the Co:Zn:Fe molar ratio was fixed to 0.5:0.5:2. Then, the pH was adjusted to 12.5 by adding NaOH solution dropwise in the mixture with constant stirring. Accompanied with continuous stirring, the solution was heated at 60 ℃ for 2 h. The co-precipitated powder was filtered and washed for several times with distilled water till the pH reached 7, and then it was dried in an oven in air atmosphere at 90 ℃ for 24 h. Finally, the powder was calcined in air at 500 ℃ for 4 h. The crystalline size of $Co_{0.5}Zn_{0.5}Fe_2O_4$ nanoparticles obtained by X-ray diffraction (XRD) and transmission electron microscopy (TEM) measurements was about 5–8 nm.

$(Co_{0.5}Zn_{0.5}Fe_2O_4)_x/Cu_{0.5}Tl_{0.5}Ba_2Ca_2Cu_3O_{10-\delta}$ superconductor samples, with $x = 0.00$, 0.04, 0.08, 0.12, 0.16, and 0.20 wt%, were prepared by single step solid-state reaction technique. Stoichometric amounts of high purity oxides of Tl_2O_3, BaO_2, CaO, and CuO were

mixed, grinded, and sifted twice by a 125 μm sieve to insure a perfectly homogenous mixture. $Co_{0.5}Zn_{0.5}Fe_2O_4$ nanoparticles were added to this powder and mixed carefully to obtain a homogenous mixture. The powder was pressed with 15 ton/cm^2 pressure using a hydraulic press to reduce the number of voids in the sample and to minimize the inter-grain contact problems. The resultant disc was 1.5 cm in diameter and about 0.3 cm in thickness. The pellets were wrapped in a silver foil in order to reduce thallium evaporation. The samples were heated inside a Muffle furnace to 760 ℃ at a rate of 4 ℃/min, followed by a rate of 2 ℃/min to 850 ℃, and finally held at this temperature for 5 h. The samples were then slowly cooled to room temperature. The samples were characterized using XRD and the results showed that the relative volume fraction for $Cu_{0.5}Tl_{0.5}$-1223 phase increases by increasing the addition of $Co_{0.5}Zn_{0.5}Fe_2O_4$ nanoparticles up to $x = 0.08$ wt% and then it decreases for further increase in x. Moreover, the lattice parameters a and c are unchanged with the increase in x.

The electrical resistivity of the prepared samples was measured from room temperature down to zero-resistivity temperature T_0 with a closed cryogenic refrigeration system. The temperature of the samples was monitored by a chromel versus Fe–Au thermocouple and stabilized with the aid of a temperature controller within ±0.1 K.

3 Results and discussion

The temperature dependence of the electrical resistivity for $(Co_{0.5}Zn_{0.5}Fe_2O_4)_x/Cu_{0.5}Tl_{0.5}$-1223 phase with $x =$ 0.00, 0.04, 0.08, 0.12, 0.16, and 0.20 wt% is displayed in Fig. 1. All the samples are characterized by a nearly sharp resistive transition, indicating the high purity of these samples. Moreover, they show a metal-like behavior in normal state, followed by a superconducting transition by decreasing temperature. The metallic behavior above T_c could be interpreted by the liquid model that provides a natural explanation for anomalous features of transport data in several HTSCs. Few models concern the linear temperature dependence of the electrical resistivity. One may exclude the electron–phonon interaction because of the relatively small electron–phonon coupling constant estimated from the electrical resistivity measurements. It is well known that the in-plane electrical resistivity is produced by the scattering of the bosons from fermions, resulting

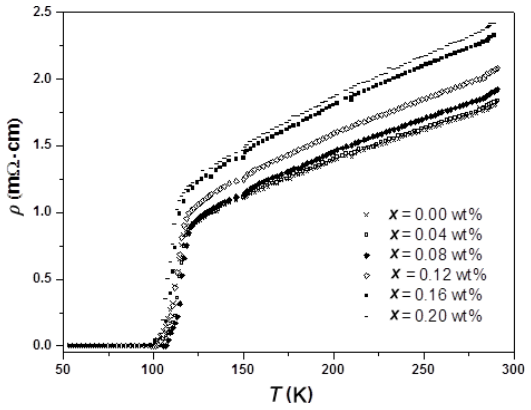

Fig. 1 Temperature dependence of the electrical resistivity for $(Co_{0.5}Zn_{0.5}Fe_2O_4)_x/Cu_{0.5}Tl_{0.5}$-1223 phase with $x = 0.00$, 0.04, 0.08, 0.12, 0.16, and 0.20 wt%.

in the linear temperature dependence. According to this model, the spin charge separation in CuO_2 planes results in two different rates, a transverse rate which gives the Hall angle dependence and the other rate is a longitudinal rate that gives the well-known linear resistivity. In addition, a small curvature in the electrical resistivity data above the superconducting transition temperature is observed. This curvature characterizes the superconducting thermodynamic (or Cooper pair) fluctuations [21] or the opening of spin gap that appears in HTSCs due to magnetic impurities [22].

The variation of room temperature resistivity ρ_{room} and residual resistivity ρ_0 with different addition of $Co_{0.5}Zn_{0.5}Fe_2O_4$ nanoparticles for $Cu_{0.5}Tl_{0.5}$-1223 phase is shown in Fig. 2. ρ_{room} is the resistivity at 300 K and ρ_0 is obtained from the fitting of resistivity data in the temperature range $170\,\text{K} \leqslant T \leqslant 300\,\text{K}$, according to Matthiessen's rule:

$$\rho_n = \rho_0 + \beta T \tag{1}$$

It is evident that both ρ_{room} and ρ_0 increase as x increases. The normal-state resistivity ρ_n is regarded as a measure of disorder, indicating that the disorder increases as x increases. It is well known that the residual resistivity arises from the impurity scattering in the CuO_2 plane. The increase in ρ_0 as x increases implies that the impurity scattering in the CuO_2 plane also increases. A similar result was observed by Nadeem *et al*. [11] for $(NiFe_2O_4)_x/Cu_{0.5}Tl_{0.5}$-1223 composite. The increase in ρ_{room} and ρ_0 is attributed to the scattering of carriers across the agglomerated magnetic nanoparticles at grain boundaries. The resistivity temperature coefficient β increases from 0.0048 to 0.0065 mΩ·cm·K^{-1} as x increases from 0.00 to 0.20 wt%. This could be due to the unsuspected

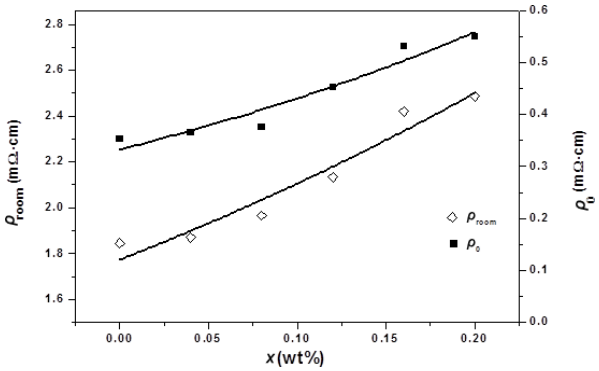

Fig. 2 Variation of room temperature resistivity ρ_{room} and residual resistivity ρ_0 with different $Co_{0.5}Zn_{0.5}Fe_2O_4$ nanoparticle addition into $Cu_{0.5}Tl_{0.5}$-1223 phase.

temperature-dependent scattering of magnetic impurities in $Co_{0.5}Zn_{0.5}Fe_2O_4$ nanoparticles [23].

3. 1 Pseudogap

The pseudogap temperature T^* is determined by plotting $d\rho/dT$ versus T and ρ_m–ρ_n versus T, where ρ_m is the measured resistivity [24]. Figures 3 and 4 show the variation of experimental resistivity and the fitted data according to Eq. (1) with temperature for $(Co_{0.5}Zn_{0.5}Fe_2O_4)_x/Cu_{0.5}Tl_{0.5}$-1223 phase for $x = 0.00$ and 0.04 wt%, respectively, and the insets of Figs. 3 and 4 show the variation of both $d\rho/dT$ and ρ_m–ρ_n with temperature. The deviation point of linear resistivity behavior with temperature is called "pseudogap temperature" which corresponds to the opening of pseudogap. There are two characteristic temperatures related to phase transition in HTSCs [25]. The first one is the pseudogap temperature T^* below which the fermions become paired. The second is the Bose–Einstein condensation temperature T_{BE} below which the bosons (responsible for conductivity) condense for the under-doped material. Since bosons are solely scattered by fermions, the decrease of scattering centering with fermions is due to the fermions pairing which causes the reduction in the electrical resistivity below the pseudogap temperature. This explains the deviation from the linear behavior of resistivity versus temperature, as observed in experiments. This separation of spin and charge is supposed to occur in 2D electron systems [26,27]. Two values for T^* are deduced from graphs $d\rho/dT$ versus temperature and ρ_m–ρ_n versus temperature. The difference between the two values is in the range of 2–6 K. Table 1 lists the average value of T^* with x. This temperature equals to T_c around optimum doping, but it is larger than T_c in the under-doped region. It is clear

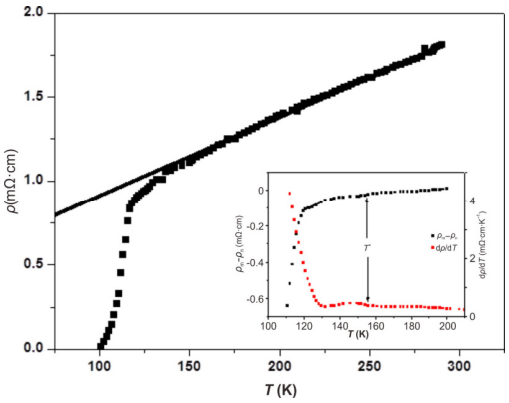

Fig. 3 Variation of resistivity with temperature for $Cu_{0.5}Tl_{0.5}$-1223 sample. The inset shows the variation of both $d\rho/dT$ and ρ_m–ρ_n with temperature.

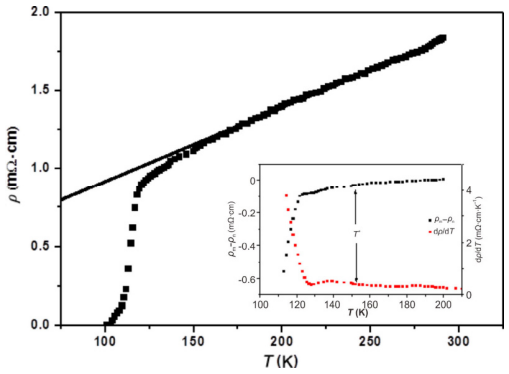

Fig. 4 Variation of resistivity with temperature for $(Co_{0.5}Zn_{0.5}Fe_2O_4)_{0.04wt\%}/Cu_{0.5}Tl_{0.5}$-1223 sample. The inset shows the variation of both $d\rho/dT$ and ρ_m–ρ_n with temperature.

Table 1 Variation of T^*, T_{scf}, T_c, ΔT_c, and ΔT_{scf} with different $Co_{0.5}Zn_{0.5}Fe_2O_4$ nanoparticle addition into $Cu_{0.5}Tl_{0.5}$-1223 phase

x (wt%)	T^* (K)	T_{scf} (K)	T_c (K)	ΔT_c (K)	ΔT_{scf} (K)
0.00	158	149	112.00	12.25	37.00
0.04	154	143	114.50	11.00	28.50
0.08	152	141	115.75	10.25	25.25
0.12	156	147	113.25	12.25	33.75
0.16	160	144	111.00	12.50	33.00
0.20	163	145	110.13	15.38	34.87

that the highest value of T_c is corresponding to the lowest value of T^*. This indicates that T^* is affected by the oxygen content or the scattering of carriers at grain boundaries. Moreover, it depends on the change of carrier density in the CuO_2 planes. This result is similar to that obtained by François *et al*. [28] for Pr-doping and oxygen deficiency on the complex conductivity and scattering rate of $YBa_2Cu_3O_{7-\delta}$ thin film, as well as Mohammadizadeh *et al*. [25] for pseudogap study in Gd-123 phase substituted by Pr. This variation between T^* and T_c could be interpreted by Emery *et al*. [29] who

have developed a preformed pair model based on micro stripes. Phase separation takes place on a microscopic scale generating dynamical charged stripes which are separated by insulating antiferromagnetic stripes.

The hole carrier concentration per Cu ion (P) is calculated through following relation [30]:

$$P = 0.16 - \left[\left(1 - \frac{T_c}{T_c^{max}}\right) / 82.6\right]^{0.5} \quad (2)$$

where T_c^{max} is taken as 120 K for $Cu_{0.5}Tl_{0.5}$-1223 phase [31]. Figure 5 shows the variation of T^* with P. An empirical relation $T^* = aP^{-b}$ yields values of a and b 27.3 and 0.86, respectively. The value of b is greater than that obtained for $Tl_2Ba_2Ca_{1-x}Y_x(Cu_{1-y}Co_y)_2O_{8+\delta}$ phase (b = 0.55–0.69) [32].

The superconducting fluctuation temperature T_{scf} is determined by analyzing the second derivative of resistivity with temperature $d^2\rho/dT^2$ [24]. Figure 6 shows the variation of $d^2\rho/dT^2$ as a function of T for $(Co_{0.5}Zn_{0.5}Fe_2O_4)_x/Cu_{0.5}Tl_{0.5}$-1223 composite with x = 0.00, 0.08, 0.12, and 0.20 wt%. T^* and T_{scf} have been estimated from $d^2\rho/dT^2$ versus T for (Hg,Re)-1223

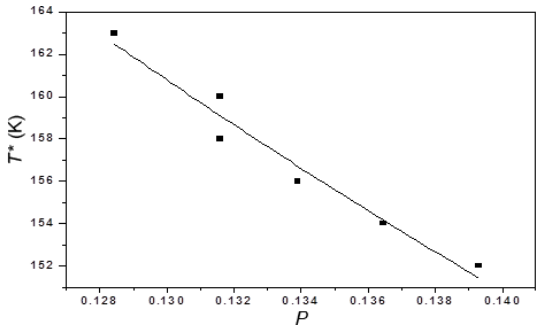

Fig. 5 Variation of T^* with P for $(Co_{0.5}Zn_{0.5}Fe_2O_4)_x$/$Cu_{0.5}Tl_{0.5}$-1223 phase.

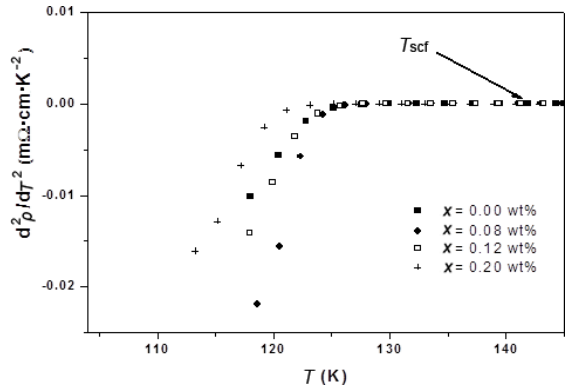

Fig. 6 Variation of $d^2\rho/dT^2$ versus T for $(Co_{0.5}Zn_{0.5}Fe_2O_4)_x/Cu_{0.5}Tl_{0.5}$-1223 composite with x = 0.00, 0.08, 0.012, and 0.20 wt%.

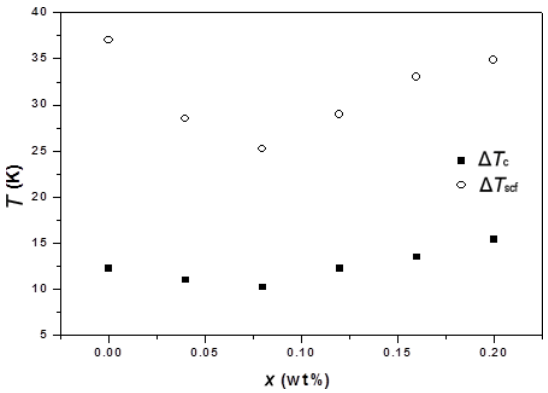

Fig. 7 Variation of both ΔT_c and ΔT_{scf} with x.

phase by Passos *et al*. [33]. $d^2\rho/dT^2$ increases in the negative region to zero and then changes its sign at which T_{scf} can be determined. There is a decrease in the superconducting fluctuation temperature T_{scf} from 149 to 141 K as x increases from 0.00 to 0.08 wt%, then it increases to 145 K for x = 0.20 wt%. It is noticed that T_{scf} lies between the superconducting transition temperature T_c and the pseudogap temperature T^*. The variation of ΔT_c ($T_c - T_0$) and ΔT_{scf} ($T_{scf} - T_c$) versus x is shown in Fig. 7. It is clear that the variation of ΔT_c and ΔT_{scf} with x has the same trend. This means that both ΔT_c and ΔT_{scf} are strongly dependent on the percolative effect and larger contributions from the grain boundaries.

3.2 Excess-conductivity

The excess-conductivity $\Delta\sigma$ is defined as

$$\Delta\sigma = \sigma_m(T) - \sigma_n(T) = \frac{\rho_n(T) - \rho_m(T)}{\rho_m(T)\rho_n(T)} \quad (3)$$

where $\rho_m(T)$ is the measured resistivity and $\rho_n(T)$ is the normal-state electrical resistivity which is calculated from Eq. (1). The normalized excess-conductivity $\frac{\Delta\sigma}{\sigma_{room}}$ is calculated by Aslamazov–Larkin (AL) [6], using a microscopic approach in the mean field region (MFR) where the fluctuations are small through the following relation:

$$\frac{\Delta\sigma}{\sigma_{room}} = At^{\alpha} \quad (4)$$

where t is the reduced temperature $t = \frac{T - T_c}{T_c}$. The superconducting transition temperature T_c is determined from the curve of $d\rho/dT$ with T and α is the conductivity exponent and expressed as

$$\alpha = \begin{cases} -0.3, \text{ cr fluctuation} \\ -0.5, \text{3D fluctuation} \\ -1.0, \text{2D fluctuation} \\ -3.0, \text{sw fluctuation} \end{cases} \quad (5)$$

A is the temperature independent amplitude and given by

$$A = \begin{cases} \dfrac{e^2}{32\hbar\xi_c(0)\sigma_{room}}, \text{ 3D region} \\ \dfrac{e^2}{16\hbar d\sigma_{room}}, \quad \text{2D region} \end{cases} \quad (6)$$

Figures 8 and 9 show the variation of $\ln\left(\dfrac{\Delta\sigma}{\sigma_{room}}\right)$ with $\ln t$ for $(Co_{0.5}Zn_{0.5}Fe_2O_4)_x/Cu_{0.5}Tl_{0.5}$-1223 phase with $x = 0.00$ and 0.08 wt%, respectively. The different fluctuation regions, sw, 2D, 3D, and cr, are clearly observed from the linear fitting, and the conductivity exponent values are determined from these slopes. The first region is observed at a temperature much higher than the mean field temperature (T_{mf}). In this temperature region, the excess-conductivity decreases sharply and agrees well with the theoretical results. The conductivity exponent α_{sw} varies from –3.1 to –2.9, in consistent with the theoretical approach. A crossover between short wave fluctuations and mean field region is observed at a temperature above T_c by decreasing temperature. The mean field region consists of two distinct linear parts. The first one is at higher temperature around $1.165T_c$. The conductivity exponent α_{2D} varies from –1.1 to –0.97, in consistent with the theoretical approach. As the temperature is lowered down to $1.08T_c$, the 3D fluctuation region appears with the conductivity exponent α_{3D} varying from –0.6 to –0.48. The 3D–2D crossover could be explained according to the high anisotropy of HTSCs, where the charge carriers move more readily in some directions than in the others. The charge carriers also show some ability to move along molecular planes in this range of thermal fluctuations. At lower temperature a crossover takes place, where the charge carriers may move between the molecular planes and cross over from one plane to another. This crossover takes place in 3D, and then the charge carriers are more affected by thermal fluctuations. This means that the charge carriers tend to move more freely in the whole crystal before they make pairs. The last region is at Ginzburg temperature $T_G = 1.01T_c$ which represents a crossover between 3D fluctuation and critical fluctuation. The value of conductivity exponent α_{cr} varies from –0.37 to –0.31, expecting from the prediction of the 3D–*xy* universality dynamics class. This could be represented by E-model [34]. The model is based on the coupling of a 2D superconducting order parameter with a symmetry-breaking field (SBF). In the critical region, below T_G, the fluctuations in the order parameter become the same magnitude as the order parameter itself [35], and the Ginzburg–Landau theory becomes unsuitable. It is well known that T_G is very close to superconducting transition temperature T_c. This means the fluctuation in the order parameter is quiet similar to superconducting carrier concentration n_s, indicating that all normal carriers converted to superconducting carriers with thermal equilibrium and fluctuation are completely disappeared.

Table 2 displays the variation of conductivity exponents α_{cr}, α_{3D}, α_{2D}, and α_{sw} and the crossover

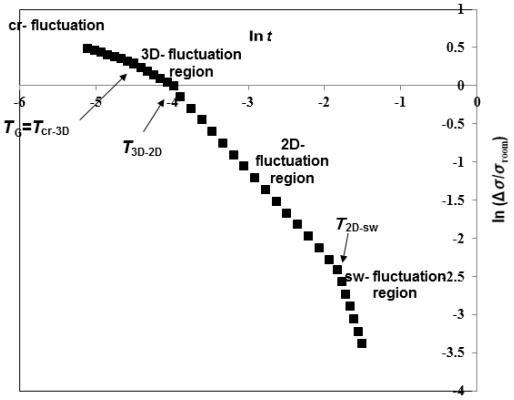

Fig. 8 Variation of $\ln\left(\dfrac{\Delta\sigma}{\sigma_{room}}\right)$ versus $\ln t$ of $Cu_{0.5}Tl_{0.5}$-1223 sample.

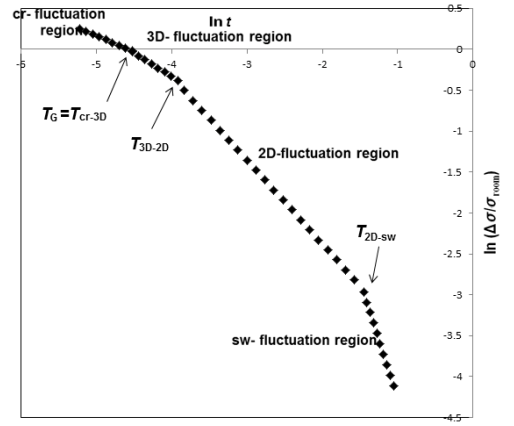

Fig. 9 Variation of $\ln\left(\dfrac{\Delta\sigma}{\sigma_{room}}\right)$ versus $\ln t$ of $(Co_{0.5}Zn_{0.5}Fe_2O_4)_{0.08wt\%}/Cu_{0.5}Tl_{0.5}$-1223 sample.

Table 2 Variation of conductivity exponents α_{cr}, α_{3D}, α_{2D}, and α_{sw} and the crossover temperatures T_{cr-3D}, T_{3D-2D}, and T_{2D-sw} with different $Co_{0.5}Zn_{0.5}Fe_2O_4$ nanoparticle addition into $Cu_{0.5}Tl_{0.5}$-1223 phase

x (wt%)	α_{cr}	α_{3D}	α_{2D}	α_{sw}	T_{cr-3D} (K)	T_{3D-2D} (K)	T_{2D-sw} (K)
0.00	–0.32	–0.61	–1.12	–3.16	113.25	115.75	128.25
0.04	–0.31	–0.53	–0.99	–3.08	115.75	116.38	136.00
0.08	–0.33	–0.48	–0.97	–3.06	117.00	118.25	139.50
0.12	–0.37	–0.61	–1.03	–2.90	114.50	115.13	135.00
0.16	–0.33	–0.54	–0.98	–2.97	112.94	114.50	129.50
0.20	–0.37	–0.61	–1.01	–2.92	111.38	112.00	124.50

temperatures T_{cr-3D}, T_{3D-2D}, and T_{2D-sw} versus the addition of $Co_{0.5}Zn_{0.5}Fe_2O_4$ nanoparticles. The crossover temperatures T_{cr-3D}, T_{3D-2D}, and T_{2D-sw} shift to higher temperatures by increasing $Co_{0.5}Zn_{0.5}Fe_2O_4$ nanoparticle addition up to $x = 0.08$ wt%, while a reverse trend is observed for $x > 0.08$ wt%. The shift of these regions to lower temperatures for $x > 0.08$ wt% indicates that the increase in $Co_{0.5}Zn_{0.5}Fe_2O_4$ nanoparticle addition into $Cu_{0.5}Tl_{0.5}$-1223 phase suppresses the phonon population [36]. This leads to the decrease of their density essential for the electron–phonon interactions, resulting in a suppression of the critical region and hence shifting these regions to lower temperatures.

The thermodynamic critical field $B_c(0)$ is estimated from the Ginzburg number N_G according to the equation:

$$N_G = \left|\frac{T_G - T_c}{T_c}\right| = \left(\frac{k_B}{B_c^2(0)\gamma^2\xi_c^3(0)}\right)^2 \quad (7)$$

where $\gamma = \frac{\xi_{ab}}{\xi_c}$ is the anisotropy parameter. The penetration depth $\lambda(0)$, lower critical magnetic field $B_{c1}(0)$, upper critical magnetic field $B_{c2}(0)$, critical current density $J_c(0)$, and Fermi energy E_F are calculated by the Ginzburg number N_G, using these following relations, respectively:

$$\lambda(0) = \frac{\varnothing_0}{2\sqrt{2}\pi B_c \xi_c(0)} \quad (8)$$

$$B_{c1}(0) = \frac{B_c}{\kappa\sqrt{2}}\ln\kappa \quad (9)$$

$$B_{c2}(0) = \sqrt{2}\kappa B_c(0) \quad (10)$$

$$J_c(0) = \frac{4\kappa B_{c1}}{3\sqrt{3}\lambda(0)\ln\kappa} \quad (11)$$

$$E_F = \frac{1}{2}m^* v_F^2 = \frac{1}{2}m^*\left(\frac{3.5\pi\xi_c(0)k_B T_c}{2\hbar}\right)^2 \quad (12)$$

where $\varnothing_0 = \frac{h}{2e}$ is the flux-quantum number, $\kappa = \frac{\lambda(0)}{\xi_c(0)}$ is the Ginzburg–Landau parameter, m^* is the effective mass of carriers ($m^* \approx 10m_e$) [37], and v_F is the Fermi velocity of carriers. These parameters are listed in Table 3 with different values of $Co_{0.5}Zn_{0.5}Fe_2O_4$ nanoparticle addition. The value of $\xi_c(0)$ for pure sample is higher than that reported by Khurram *et al*. ($\xi_c(0) = 10$ Å) [38]. These results could be interpreted according to the simple grain model. Ceramic samples exhibit complex transport behavior because they are composed of crystallites, in which the transport depends on the mixing of the conductor planes (*ab*) with the insulating *c*-axis, the inhomogeneity, and the nature of present defects at the crystalline boundaries. $\xi_c(0)$ decreases as x increases from 0.00 to 0.08 wt% and then it increases with further increase in x for $(Co_{0.5}Zn_{0.5}Fe_2O_4)_x/Cu_{0.5}Tl_{0.5}$-1223 phase. The increase in $\xi_c(0)$ could be attributed to the removal of oxygen from the charge reservoir layer. All the values of inter-layer coupling are less than one, indicating a weak coupling between the CuO_2 planes [39]. The thermodynamic critical field, lower critical field, upper critical field, and critical current density increase as x increases from 0.0 to 0.08 wt%; beyond that they decrease with further increase in x. This means that the addition of $Co_{0.5}Zn_{0.5}Fe_2O_4$ nanoparticles improves the superconducting parameters, while the high addition of $Co_{0.5}Zn_{0.5}Fe_2O_4$ nanoparticles degrades them. The increase in thermodynamic parameters $B_c(0)$, $B_{c1}(0)$, $B_{c2}(0)$, and $J_c(0)$ could be due to the reduction of magnetic vortex motion via improvement of pinning capability within the sample, suggesting the presence of strong pinning sources. Snezhko *et al*. [40] found that the enhancement of vortex pinning by the addition of magnetic nanoparticles in the bulk type-II superconductors is due to the interaction between the finite-size spherical magnetic inclusion and Abrikosov vortex. Moreover, they showed that the magnetic nanoparticles lead to a considerable enhancement of vortex pinning in large κ type-II superconductors. On the other hand, the decrease in the superconducting parameters is attributed to the increase in the grain boundary resistance, the formation of secondary phases, and the reduction in the flux pinning inside the samples. The calculated Fermi velocities for all prepared samples are found to be less than that of the free electron ($v_F = 10^6$ m·s^{-1}), and the Fermi energy decreases as x increases from 0.00 to 0.08 wt%, then it increases with

further increase in x. The enhancement of E_F with the increase in x is probably due to the change in the band structure of carriers or the change of carrier concentration in CuO_2 plane. Finally, one can notice that the values of $B_c(0)$, $B_{c2}(0)$, and E_F are nearly close to those obtained for $Cr_x/Cu_{0.5}Tl_{0.5}$-1223 [10] and $(NiFe_2O_4)_x/Cu_{0.5}Tl_{0.5}$-1223 [11] phases, while the values of $\xi_c(0)$ are greater than those reported by Qasim *et al*. [10] and Nadeem *et al*. [11]. Moreover, the values of $J_c(0)$ are greater than those reported by Qasim *et al*. [10]. This difference is probably due to the different preparation methods and calculation method of $\xi_c(0)$. On the other hand, the values of $\xi_c(0)$ are quite similar to that reported by Abou-Aly *et al*. [41] for $Cu_{0.5}Tl_{0.5}$-1223 phase.

4 Conclusions

Composite superconducting samples of type $(Co_{0.5}Zn_{0.5}Fe_2O_4)_x/Cu_{0.5}Tl_{0.5}$-1223 were successfully prepared by solid-state reaction technique. The electrical resistivity behavior above T_c was investigated using pseudogap and excess-conductivity analysis in order to determine the superconducting parameters. The pseudogap temperature was related to T_c and the hole carrier concentration; it was decreased by increasing them. The variation of ΔT_c and ΔT_{scf} with x had the same trend, indicating that they were strongly dependent on the percolative effect and larger contributions from the grain boundaries, respectively. It was found that, from excess-conductivity analysis, the thermodynamic parameters were improved by increasing $Co_{0.5}Zn_{0.5}Fe_2O_4$ nanoparticle addition up to $x = 0.08$ wt%, beyond which they were deteriorated for $Cu_{0.5}Tl_{0.5}$-1223 phase. This improvement could be explained according to the enhancement in vortex pinning through the addition of magnetic $Co_{0.5}Zn_{0.5}Fe_2O_4$ nanoparticles into $Cu_{0.5}Tl_{0.5}$-1223 phase, resulting from the interaction of finite-size spherical magnetic inclusion with Abrikosov vortex.

Acknowledgements

This work was performed in the Superconductivity and Metallic Glass Lab, Physics Department, Faculty of Science, Alexandria University, Alexandria, Egypt, in collaboration with Beirut Arab University, Beirut, Lebanon.

References

[1] Tokiwa K, Tanaka Y, Iyo A, *et al*. High pressure synthesis and characterization of single crystals of $CuBa_2Ca_3Cu_4O_y$ superconductor. *Physica C* 1998, **298**: 209–216.

[2] Takeuchi T, Iijima Y, Inoue K, *et al*. Effect of flat-roll forming on critical current density characteristics and microstructure of Nb_3Al multifilamentary conductors. *IEEE T Appl Supercon* 1997, **7**: 1529–1532.

[3] Ihara H. New low anisotropic high-T_c superconductors (Cu, Ag)$Ba_2Ca_{n-1}Cu_nO_{2n+4-y}$. In *Advances in Superconductivity VII*. Yamafuji K, Morishita T, Eds. Springer Japan, 1995: 255–260.

[4] Ihara H, Sekita Y, Tateai H, *et al*. Superconducting properties of $Cu_{1-x}Tl_x$-1223 $[Cu_{1-x}Tl_x(Ba,Sr)_2Ca_2Cu_3O_{10-y}]$ thin films. *IEEE T Appl Supercon* 1999, **9**: 1551–1554.

[5] Khan NA, Sekita Y, Tateai F, *et al*. Preparation of biaxially oriented TlCu-1234 thin films. *Physica C* 1999, **320**: 39–44.

[6] Aslamazove LG, Larkin AI. The influence of fluctuation pairing of electrons on the conductivity of normal metal. *Phys Lett A* 1968, **26**: 238–239.

[7] Thompson RS. Microwave, flux flow, and fluctuation resistance of dirty type-II superconductors. *Phys Rev B* 1970, **1**: 327.

[8] Lawrence WE, Doniach S. Theory of layer structure superconductor. In Proceedings of the 12th International Conference on Low-Temperature Physics. Kanda E, Ed. Keigaku, Tokyo, 1971: 361.

[9] Hikami S, Larkin AI. Magnetoresistance of high temperature superconductors. *Mod Phys Lett B* 1988, **2**: 693.

Table 3 Variation of the calculated superconducting parameters with different $Co_{0.5}Zn_{0.5}Fe_2O_4$ nanoparticle addition into $Cu_{0.5}Tl_{0.5}$-1223 phase

x (wt%)	N_G	$\xi_c(0)$ (Å)	J	d (Å)	$B_c(0)$	$B_{c1}(0)$	$B_{c2}(0)$	J_c (10^3A·cm^{-2})	λ (Å)	κ	v_F (10^5m·s^{-1})	E_F (eV)
0.00	0.0111	16.57	0.019	235.54	2.22	0.24	119.97	3.71	326.40	19.696	1.35	0.13
0.04	0.0109	14.35	0.016	220.74	2.77	0.28	159.98	5.00	302.08	21.049	1.19	0.10
0.08	0.0107	13.16	0.014	216.99	3.16	0.31	190.05	5.97	288.57	21.916	1.10	0.08
0.12	0.0110	22.54	0.035	240.75	1.40	0.16	64.82	2.01	379.68	16.839	1.85	0.24
0.16	0.0083	26.72	0.044	252.56	1.16	0.15	46.14	1.64	385.68	14.432	2.17	0.34
0.20	0.0113	28.71	0.044	273.02	0.97	0.12	39.96	1.22	431.49	15.026	2.29	0.38

[10] Qasim I, Waqee-ur-Rehman M, Mumtaz M, *et al*. Role of anti-ferromagnetic Cr nanoparticles in CuTl-1223 superconducting matrix. *J Alloys Compd* 2015, **649**: 320–326.

[11] Nadeem K, Hussain G, Mumtaz M, *et al*. Role of magnetic $NiFe_2O_4$ nanoparticles in CuTl-1223 superconductor. *Ceram Int* 2015, **41**: 15041–15047.

[12] Hussain G, Jabbar A, Qasim I, *et al*. Activation energy and excess conductivity analysis of $(Ag)_x$/CuTl-1223 nano-superconductor composites. *J Appl Phys* 2014, **116**: 103911.

[13] Naqib SH. Effects of Zn on superconductivity, stripe order, and pseudogap correlations in $YBa_2(Cu_{1-y}Zn_y)_3O_{7-\delta}$. *Physica C* 2012, **476**: 10–14.

[14] Emery VJ, Kivelson SA. Importance of phase fluctuations in superconductors with small superfluid density. *Nature* 1994, **374**: 434–437.

[15] Chen Q, Kosztin I, Jankó B, *et al*. Pairing fluctuation theory of superconducting properties in underdoped to overdoped cuprates. *Phys Rev Lett* 1998, **81**: 4708.

[16] Chubukov AV, Schmalian J. Temperature variation of the pseudogap in underdoped cuprates. *Phys Rev B* 1998, **57**: R11085.

[17] Anderson PW. The 'spin gap' in cuprate superconductors. *J Phys: Condens Matter* 1996, **8**: 10083.

[18] Lee PA. Pseudogaps in underdoped cuprates. *Physica C* 1999, **317–318**: 194–204.

[19] Tallon JL, Loram JW. The doping dependence of T^*—what is the real high-T_c phase diagram? *Physica C* 2001, **349**: 53–68.

[20] Khurram AA, Khan NA, Mumtaz M. Intercomparison of fluctuation induced conductivity of $Cu_{0.5}Tl_{0.5}Ba_2Ca_{n-1}Cu_nO_{2n+4-y}$ ($n = 2$, 3, 4) superconductor thin films. *Physica C* 2009, **469**: 279–282.

[21] Abou Aly AI, Ibrahim IH, Awad R, *et al*. Stabilization of Tl-1223 phase by arsenic substitution. *J Supercond Nov Magn* 2010, **23**: 1325–1332.

[22] Koo JH, Cho G. The spin-gap in high T_c superconductivity. *J Phys: Condens Matter* 2003, **15**: L729.

[23] Abou-Aly AI, Awad R, Ibrahim IH, *et al.* Excess conductivity analysis for $Tl_{0.8}Hg_{0.2}Ba_2Ca_2Cu_3O_{9-\delta}$ substituted by Sm and Yb. *Solid State Commun* 2009, **149**: 281–285.

[24] Naqib SH, Cooper JR, Tallon JL, *et al*. Doping phase diagram of $Y_{1-x}Ca_xBa_2(Cu_{1-y}Zn_y)_3O_{7-\delta}$ from transport measurements: Tracking the pseudogap below T_c. *Phys Rev B* 2005, **71**: 054502.

[25] Mohammadizadeh MR, Akhavan M. Pseudogap in Gd-based 123 HTSC. *Physica B* 2003, **336**: 410–419.

[26] Anderson PW. The resonating valence bond state in La_2CuO_4 and superconductivity. *Science* 1987, **235**: 1196–1198.

[27] Lee PA, Nagaosa N, Ng T-K, *et al.* SU(2) formulation of the t–J model: Application to underdoped cuprates. *Phys Rev B* 1998, **57**: 6003.

[28] François I, Jaekel C, Kyas G, *et al*. Influence of Pr doping and oxygen deficiency on the scattering behavior of $YBa_2Cu_3O_7$ thin films. *Phys Rev B* 1996, **53**: 12502.

[29] Emery VJ, Kivelson SA, Zachar O. Spin-gap proximity effect mechanism of high-temperature superconductivity. *Phys Rev B* 1997, **56**: 6120.

[30] Presland MR, Tallon JL, Buckley RG, *et al.* General trends in oxygen stoichiometry effects on T_c in Bi and Tl superconductors. *Physica C* 1991, **176**: 95–105.

[31] Ihara H, Tanaka K, Tanaka Y, *et al.* Mechanism of T_c enhancement in $Cu_{1-x}Tl_x$-1234 and -1223 system with $T_c >$ 130 K. *Physica C* 2000, **341–348**: 487–488.

[32] Poddar A, Bandyopadhyay B, Chattopadhyay B. Effects of Co-substitution on superconductivity and transport in $Tl_2Ba_2Ca_{1-x}Y_x(Cu_{1-y}Co_y)_2O_{8+\delta}$. *Physica C* 2003, **390**: 120–126.

[33] Passos CAC, Passamai Jr. JL, Orlando MTD, *et al*. An investigation of T^* behavior on (Hg,Re)-1223 system. *Physica C* 2007, **460–462**: 1086–1087.

[34] Hohenberg PC, Halperin BI. Theory of dynamic critical phenomena. *Rev Mod Phys* 1977, **49**: 435.

[35] Lobb CJ. Critical fluctuations in high-T_c superconductors. *Phys Rev B* 1987, **36**: 3930.

[36] Rahim M, Khan NA. Suppressed phonon density and Para conductivity of Cd doped $Cu_{0.5}Tl_{0.5}Ba_2Ca_3Cu_{4-y}Cd_yO_{12-\delta}$ ($y = 0$, 0.25, 0.5, 0.75) superconductors. *J Alloys Compd* 2012, **513**: 55–60.

[37] Bardeen J, Cooper LN, Schrieffer JR. Theory of superconductivity. *Phys Rev* 1957, **108**: 1175.

[38] Khurram AA, Khan NA. A search for a low anisotropic superconductor. *J Electromagnetic Analysis & Applications* 2010, **2**: 63–74.

[39] Geru II, Ghilan ZI, Dihor IT, *et al*. *Moldavian Journal of the Physical Sciences* 2002, **N2**: 53.

[40] Snezhko A, Prozorov T, Prozorov R. Magnetic nanoparticles as efficient bulk pinning centers in type-II superconductors. *Phys Rev B* 2005, **71**: 024527.

[41] Abou-Aly AI, Awad R, Kamal M, *et al.* Excess conductivity analysis of $(Cu_{0.5}Tl_{0.5})$-1223 substituted by Pr and La. *J Low Temp Phys* 2011, **163**: 184–202.